

Decay of the superheavy nucleus  $^{310}\text{126}$ R. A. Gherghescu <sup>1</sup>, H. Stoecker <sup>2</sup>, and D. N. Poenaru<sup>1</sup><sup>1</sup>*Department for Theoretical Physics, Horia Hulubei National Institute for Physics and Nuclear Engineering, Bucharest-Magurele 077125, Romania*<sup>2</sup>*Frankfurt Institute for Advanced Studies, Riedberg Campus, Ruth-Moufang Straße 1, D-60438 Frankfurt am Main, Germany*

(Received 14 November 2023; accepted 23 January 2024; published 15 February 2024)

There are three accepted next proton closures beyond the lead atomic number:  $Z = 114$ ,  $120$ , and  $126$ . The heaviest one,  $Z = 126$ , is analyzed within its decay process. A binary adapted macroscopic-microscopic method is used to obtain all fission barriers along different decay channels. The whole range of mass asymmetry is calculated for the fragment emission. The deformed two-center shell model is used to obtain the proton and neutron single-particle energy levels. The levels are used as input for the shell correction energy. The binary Yukawa-plus-exponential model leads to calculation of the macroscopic part of the deformation energy. The dynamics is completed with the Werner-Wheeler mass tensor components. The Wentzel-Kramers-Brillouin (WKB) method provides the penetrabilities and therefore the half-lives for all possible decay channels of  $^{310}\text{126}$ .

DOI: [10.1103/PhysRevC.109.024611](https://doi.org/10.1103/PhysRevC.109.024611)

## I. INTRODUCTION

Superheavy elements have now been synthesized in many laboratories all over the world. Cyclotrons at Lawrence Berkeley [1] and Flerov Laboratory [2] were among the first tools used to obtain these nuclei in heavy ion reactions. Later on, more powerful accelerators were built at GSI-Darmstadt [3,4] and RIKEN [5]. The relevance and importance were underlined in [6]. Theoretically, the macroscopic-microscopic model predicted for the first time the existence of these elements beyond uranium. The possible ground states appear as a result of proton shell closures, revealed due to the Strutinsky [7] shell correction method. Early calculations indicated three possible rather stable elements due to these closures. The first one indicated that  $Z = 114$  could be a stable nucleus compared to its neighbors. Such calculations were performed in [8,9]. Self-consistent calculations with Hartree-Fock approach using finite range (Gogny) forces predicted stability around  $^{298}\text{114}$  [10], whereas  $Z = 120$  was obtained as an energy minimum using zero-range Skyrme interactions in [11]. The occurrence of spherical shell closure in the superheavy nucleus region was studied in detail in [12] also within the relativistic Hartree-Fock-Bogoliubov theory. These detailed calculations provide  $Z = 120$  as a reliable prediction for proton closure. In the same work however,  $Z = 114$  and  $126$  are also considered as promising candidates. The last candidate for superheavy minimum energy is  $Z = 126$ . This proton closure was obtained using zero-range Skyrme forces SkP and Ly7. The same proton closure was calculated with macroscopic plus Woods-Saxon microscopic potentials in [13]. A gap in the neutron energy at  $N = 184$  was confirmed since early calculations within the macroscopic-microscopic calculations [14,15], but also by self-consistent methods [11,16] or using a semiempirical shell model mass equation [17].

Up to now, the macroscopic-microscopic method proved to be a reliable approach for the study of the stability and

decay of heavy elements. The macroscopic part is based on a deformed charged liquid drop body. The microscopic term comes as the shell corrections, basically calculated as the Strutinsky term [7]. A lot of work is dedicated to the theory of fission for superheavy elements, for example in [18–20], using the modified generalized liquid drop model, or liquid drop plus Nilsson shell model in [21], in order to compute the fission barriers. Self-consistent models like Skyrme-Hartree-Fock and relativistic mean field have been used extensively for study in the superheavy region, and have been shown to exhibit differences in their predictions concerning fission barrier heights [22]. Also fission barriers for heavy nuclei are investigated beyond the second saddle point by the constrained relativistic mean field method [23].

The alpha emission from superheavy nuclei draws special attention, in connection with the presumed stable  $Z = 126$  element. This part is related to the present work, being a good opportunity to compare calculations with experimentally detected alpha chain emission. Such theoretical calculations were performed for example in [24], using a Coulomb and proximity potential model for deformed nuclei. Again, the modified generalized liquid drop model is employed to study the heavy particle radioactivity of  $Z = 126$  [25]. As proof of the diversity of the theoretical models, the alpha-decay chain of  $^{314-340}\text{126}$  is also studied using a cubic plus proximity potential with an improved transfer matrix model in [26], but also, again, the macroscopic-microscopic method, with Yukawa potential for alpha emission, in [27].

The present work is related to the above cited publications as being an exploration of the stability and decay of the presumed doubly magic superheavy element  $^{310}\text{126}$ . The study presents a specialized binary macroscopic-microscopic method for the calculation of the typical fission quantities applied to this massive nucleus. All possible decay channels are covered, browsing the whole range of fission mass

asymmetry. Section II presents the theoretical details of the method. Section III is dedicated to the numerical results of the calculations and discussion of the fission quantities. The last section draws the principal conclusions.

## II. SPECIALIZED MACROSCOPIC-MICROSCOPIC MODEL FOR FISSION PHENOMENA

The binary macroscopic-microscopic method has been developed to assess the evolution of the nuclear shape from a single parent nucleus to two separated fission fragments. Its main characteristics allow the description of the two partially overlapped quantum systems and the smooth passage towards separated ones [28]. The total statical deformation energy  $E_b$  is obtained as the sum of the liquid drop and the microscopic energies:

$$E_b = \Delta E_{\text{mac}}^{(\text{def})} + \delta E_{\text{sh}}. \quad (1)$$

The macroscopic term  $\Delta E_{\text{mac}}^{(\text{def})}$  is built up as a charged liquid drop compensated by the surface nuclear force, being the only shape dependent classical quantities. The microscopic part consists of a binary modeled shell correction energy  $\delta E_{\text{sh}}$ , adapting the Strutinsky method to the two-nucleus system. The two overlapping quantum wells are deformed according to the shape characteristics of each fission partner at a certain point of elongation. The microscopic term is calculated separately for protons and neutrons, and the results are added. Finally the fission barrier  $E_b$  is obtained as the sum of the macroscopic and microscopic terms at each stage of the deformation evolution of the process.

$$\begin{aligned} G_{HL}(z, z') = & \left\{ \rho_H(z)\rho_L(z') \frac{K(k_{HL}) - 2D(k_{HL})}{3} \left[ 2[\rho_H^2(z) + \rho_L^2(z')] - (z - z')^2 + 1.5(z - z') \left( \frac{d\rho_H^2(z')}{dz'} - \frac{d\rho_L^2(z)}{dz} \right) \right] \right. \\ & + K(k_{HL}) \left[ \frac{\rho_H^2(z)\rho_L^2(z')}{3} + \left( \rho_H^2(z) - 0.5(z - z') \frac{d\rho_H^2(z)}{dz} \right) \left( \rho_L^2(z') + 0.5(z - z') \frac{d\rho_L^2(z')}{dz'} \right) \right] \left. \right\} \\ & \times \frac{1}{\{[\rho_H(z) + \rho_L(z')]^2 + (z - z')^2\}^{1/2}}. \end{aligned} \quad (5)$$

Here we have to mention the use of the complete elliptic integrals of first and second degree taken from [29]

$$\begin{aligned} D(k) &= K(k) - \mathcal{F}(k), \\ K(k) &= \int_0^{\pi/2} (1 - k^2 \sin^2 t)^{-1/2} dt, \\ \mathcal{F}(k) &= \int_0^{\pi/2} (1 - k^2 \sin^2 t)^{1/2} dt. \end{aligned} \quad (6)$$

The argument  $k$  is chosen so as to have the cuts on the symmetry axis at  $-1$  and  $1$ . The noninteracting terms  $F_{CH}$  and  $F_{CL}$  are easily obtained by replacing  $HL$  with heavy  $H$  and light  $L$  symbols, and the corresponding shape equations  $\rho_H(z)$  and  $\rho_L(z)$ .

### A. The deformed macroscopic Yukawa-plus-exponential energy

The doubly built Yukawa-plus-exponential potential  $\Delta E_{\text{YE}}$  plus the Coulomb one  $\Delta E_C$ , form the macroscopic energy part. Each of the terms is obtained for a deformed partner, where one adds the interaction between them. The total macroscopic deformation energy term is scaled to the spherical configuration, so that

$$\begin{aligned} \Delta E_C &= E_C - E_C^{\text{sph}}, \\ \Delta E_{\text{YE}} &= E_{\text{YE}} - E_{\text{YE}}^{\text{sph}}, \\ E_{\text{mac}}^{(\text{def})} &= \Delta E_{\text{YE}} + \Delta E_C. \end{aligned} \quad (2)$$

The Coulomb term takes into account also the different values of the charge density:

$$\Delta E_C = \frac{2\pi}{3} (\rho_{eH}^2 F_{CH} + \rho_{eL}^2 F_{CL} + 2\rho_{eH}\rho_{eL} F_{CHL}) - \frac{3Z^2 e^2}{5r_0 A^{1/3}}. \quad (3)$$

Here  $\rho_{eH}$  and  $\rho_{eL}$  are the charge densities ( $H = \text{heavy}$ ,  $L = \text{light}$ ), and  $F_{ij}$  are the shape dependent terms. The last expression accounts for the spherical Coulomb energy of the parent, as one considers  $^{310}_{126}$  doubly magic. The fragments are considered to be ellipsoidally deformed. The Coulomb interaction term  $F_{CHL}$  between the two partially overlapped fragments reads

$$F_{CHL} = \int_{-a_H}^{z_s} dz \int_{z_s}^{R+a_L} dz' G_{HL}(z, z') \quad (4)$$

where  $a_H$ ,  $a_L$  are the long semiaxes of the fragments at a certain distance between centers  $R$ . The integrand is an exclusively geometric term:

The nuclear surface term is constructed taking into account the finite range of the nuclear force. One uses the Yukawa-plus-exponential potential [30], adapted for binary shapes. Similarly to the Coulomb treatment, the nuclear surface term reads

$$\begin{aligned} \Delta E_{\text{YE}} &= E_Y^{(\text{def})} - E_Y^{(\text{sph})} \\ &= \frac{1}{4\pi r_0^2} [c_{sH} D_{Y_H} + c_{sL} D_{Y_L} + 2(c_{sH} c_{sL})^{1/2} D_{Y_{HL}}] \\ &\quad - \left\{ 1 - 3 \left( \frac{a}{R_0} \right)^2 + \left( \frac{R_0}{a} + 1 \right) \left[ 2 + 3 \frac{a}{R_0} \right. \right. \\ &\quad \left. \left. + 3 \left( \frac{a}{R_0} \right)^2 \right] \exp \left( -\frac{2R_0}{a} \right) \right\} c_s A^{2/3}, \end{aligned} \quad (7)$$

where the surface coefficients depend on the isospin of the nucleus:

$$c_{sH,L} = a_s \left[ 1 - \kappa \left( \frac{N_{H,L} - Z_{H,L}}{A_{H,L}} \right)^2 \right]. \quad (8)$$

The  $D_Y$  terms are again only shape configuration dependent. Their basic formula [31] is adapted for binary configuration of two interacting nuclei. The interaction term reads

$$D_{YHL} = \int_0^{2\pi} \int_{-a_H}^{z_s} \int_{z_s}^{R+a_L} E_{Y_H}^{(HL)} E_{Y_L}^{(HL)} Q^{(HL)} d\Phi dz dz', \quad (9)$$

where the constituents depend exclusively on the nuclear shape equation:

$$\begin{aligned} E_{Y_L}^{(H,L)} &= \rho_{H,L}^2(z) - \rho_{H,L}(z)\rho_{H,L}(z') \cos \Phi \\ &\quad - 0.5(z-z') \frac{d\rho_{H,L}^2(z)}{dz}, \\ E_{Y_H}^{(H,L)} &= \rho_{H,L}^2(z) - \rho_{H,L}(z)\rho_{H,L}(z') \cos \Phi \\ &\quad + 0.5(z-z') \frac{d\rho_{H,L}^2(z')}{dz'}, \\ Q^{(HL)} &= 2 - \left[ \left( \frac{\sigma_{H,L}}{a} \right)^2 + 2 \frac{\sigma_{H,L}}{a} - 2 \right] \\ &\quad \times \exp \left( - \frac{\sigma_{H,L}}{a} \right) \frac{1}{\sigma_{H,L}^4}. \end{aligned} \quad (10)$$

The surface strength coefficient  $\sigma_{H,L}$  reads

$$\begin{aligned} \sigma_{H,L} &= \left[ \rho_{H,L}^2(z) + \rho_{H,L}^2(z') - 2\rho_{H,L}(z)\rho_{H,L}(z') \cos \Phi \right. \\ &\quad \left. + (z-z')^2 \right]^{1/2}. \end{aligned} \quad (11)$$

In this way, through the surface equations for fission configurations  $\rho_{H,L}(z)$ , and the different strength values for the finite nuclear force  $c_{sH,L}$  and the surface dependent ones  $\sigma_{H,L}$ , as well as accounting for the different charge densities, the macroscopic energy is a binary dependent term.

## B. Microscopic corrections

The macroscopic barrier for superheavy nuclei is almost nonexistent. The Coulomb repulsion is so strong that the surface forces are overcome, hence, with only this energy, massive nuclear systems could not survive. The microscopic potential generates the single-particle levels, which provide an additional energy named shell corrections. This effect was emphasized for the first time in [7]. A binary microscopic potential has been constructed to account for this special type of quantum evolution. Such models have drawn attention since the 1970s in [32], and have been developed also under a realistic binary Woods-Saxon potential [33], also used to predict the production of superheavy elements by incomplete fusion reactions [34]. The potential constructed here,  $V_{\text{DTCSM}}$ , for the microscopic part of the binary method is based on a two-center deformed oscillators, with spin-orbit and  $\hat{l}^2$  interactions added [35], for axially symmetric shapes:

$$V_{\text{DTCSM}}(\rho, z) = V_{2\text{-osc}}(\rho, z) + V_{\hat{l}^2}(\rho, z) + V_{\hat{s}}(\rho, z), \quad (12)$$

where the two-deformed oscillators part read:

$$V_{2\text{-osc}}(\rho, z) = \begin{cases} \frac{1}{2} m_0 [\omega_{\rho_H}^2 \rho^2 + \omega_{z_H}^2 (z + z_H)^2], & (\rho, z) \in \text{vol}(A_H), \\ \frac{1}{2} m_0 [\omega_{\rho_L}^2 \rho^2 + \omega_{z_L}^2 (z - z_L)^2], & (\rho, z) \in \text{vol}(A_L). \end{cases}$$

The frequencies are related to the ellipsoidal deformations through the equipotential nuclear surface condition:

$$\frac{\omega_{\rho_{H,L}}}{\omega_{z_{H,L}}} = \frac{a_{H,L}}{b_{H,L}} \quad \text{and} \quad V_{2\text{-osc}} = V_0 = \frac{m_0 \omega_0^2 R_{H,L}^2}{2} \quad (13)$$

with  $a_{H,L}$ ,  $b_{H,L}$  being the fragment ellipsoid semiaxes, and  $R_{H,L}$  the corresponding radius of the spherical shape for the same mass. At this point the spin-orbit  $V_{\hat{l}^2}$  and  $V_{\hat{s}}$  potentials determine which proton shell will be a complete closure after  $Z = 82$ . For a considered sphere, these additional terms are

$$\begin{aligned} V_{\hat{l}^2}^{(\text{sph})} &= - \frac{\hbar}{m_0 \omega_0} \kappa \hat{l} \hat{s}, \\ V_{\hat{s}}^{(\text{sph})} &= - \frac{\hbar}{m_0^2 \omega_0^3} \kappa \mu \hat{l}^2. \end{aligned} \quad (14)$$

One can see that the force intensity coefficients  $\kappa$  and  $\mu$  are decisive in determining a local minimum of these quantities. As the shape evolves towards binary configurations, the residual interactions are obtained as

$$\begin{aligned} V_{\hat{l}^2}^{(H,L)}(\rho, z) &= - \left\{ \frac{\hbar}{m_0 \omega_{0H,L}} \kappa_{H,L}(\rho, z), [\nabla V_{2\text{-osc}}(\rho, z) \times \hat{p}] \hat{s} \right\}, \quad (\rho, z) \in \text{vol}(A_{H,L}), \\ V_{\hat{s}}^{(H,L)}(\rho, z) &= - \left\{ \frac{\hbar}{m_0^2 \omega_{0H,L}^3} \kappa_{H,L} \mu_{H,L}(\rho, z), [\nabla V_{2\text{-osc}}(\rho, z) \times \hat{p}]^2 \right\}, \quad (\rho, z) \in \text{vol}(A_{H,L}). \end{aligned} \quad (15)$$

These forms ensure the passage from the initial spherical values to the final heavy ( $H$ ) and light ( $L$ ) spin-orbit and  $\hat{l}^2$  fragment values. An anticommutator is used to ensure self-adjointness.

The total deformed two-center Hamiltonian  $H_{\text{DTCSM}}$  reads

$$H_{\text{DTCSM}}(\rho, z) = -\frac{\hbar^2}{2m_0}\Delta + V_{\text{DTCSM}}(\rho, z), \quad (16)$$

which is solved for the two-oscillator part. This leads to the binary Schrödinger equation. When solved, it provides the solutions that constitute the basis  $\{\Psi_{m,n,\rho,v}\}$  for solving the deformation dependent potentials:

$$\Psi_{m,n,\rho,v}(\phi, \rho, z) = \Phi_m(\phi)R_{n_\rho}^{|m|}(\rho)Z_v(z), \quad (17)$$

where

$$\begin{aligned} \Phi_m(\phi) &= \frac{1}{\sqrt{2\pi}} \exp(im\phi), \\ R_{n_\rho}^{|m|}(\rho) &= \left[ \frac{2\Gamma(n_\rho + 1)\alpha_H^2}{\Gamma(n_\rho + |m| + 1)} \right]^{1/2} \exp\left(-\frac{\alpha_H^2 \rho^2}{2}\right) (\alpha_H^2 \rho^2)^{\frac{|m|}{2}} L_{n_\rho}^{|m|}(\alpha_H^2 \rho^2), \\ Z_v^{(H,L)}(z) &= \begin{cases} C_{v_H} \exp\left[-\frac{\alpha_H^2(z+z_H)^2}{2}\right] \mathcal{H}_{v_H}[-\alpha_H(z+z_H)], & z \in \text{vol}(A_H) \\ C_{v_L} \exp\left[-\frac{\alpha_L^2(z-z_L)^2}{2}\right] \mathcal{H}_{v_L}[\alpha_L(z-z_L)], & z \in \text{vol}(A_L). \end{cases} \end{aligned} \quad (18)$$

The last function  $Z_v^{(H,L)}(z)$  provides the solution belonging to the heavy ( $H$ ) or light ( $L$ ) region of the potential, hence the binary character of the process. The spin-orbit  $\hat{l}\hat{s}$  and  $\hat{l}^2$  matrix operators

$$\begin{aligned} \langle l|\hat{l}\hat{s}| \rangle &= \langle \Psi_{m'n'_\rho v'} | V_{\hat{l}\hat{s}}^{(H,L)}(\rho, z) | \Psi_{m,n,\rho,v} \rangle_{\text{vol}(H,L)}, \\ \langle l|\hat{l}^2| \rangle &= \langle \Psi_{m'n'_\rho v'} | V_{\hat{l}^2}^{(H,L)}(\rho, z) | \Psi_{m,n,\rho,v} \rangle_{\text{vol}(H,L)} \end{aligned} \quad (19)$$

provide, after diagonalization within the  $\{\Psi_{m,n,\rho,v}\}$  basis, the residual energies for each region of the fissionlike configuration, and, further on, the single-particle schemes at every stage of elongation. Once the level schemes are obtained, the single-particle energies are input data for the Strutinsky method to obtain the final shell corrections [7]. The stable state of the parent is ensured by a strong negative value of this quantity, which in turn comes out when searching for the most stable state of the spherical nucleus. The spin-orbit and  $\hat{l}^2$  operators provide this energy minimum by finding the appropriate strength parameters  $\kappa$  and  $\mu$ . The Strutinsky method is repeated for protons,  $E_{\text{shp}}$ , and neutrons,  $E_{\text{shn}}$ , independently and the results are summed:

$$\delta E_{\text{sh}} = E_{\text{shp}} + E_{\text{shn}}, \quad (20)$$

where

$$E_{\text{shp,shn}} = \sum_{v=1}^n 2E_{v,p,n} - \tilde{U}_{p,n}. \quad (21)$$

The first term is the sum of the proton/neutron single particle energy levels, whereas  $\tilde{U}_{p,n}$  is the so-called smoothed distribution energy. This term is calculated by considering the level scheme as being uniformly distributed with a level density of [36]

$$\tilde{g}(\epsilon) = \int_{-\infty}^{\infty} \zeta\left(\frac{\epsilon - \epsilon'}{\gamma}\right) g(\epsilon') d\epsilon' = \frac{1}{\gamma} \sum_i \zeta\left(\frac{\epsilon - \epsilon_i}{\gamma}\right), \quad (22)$$

where  $\gamma \approx \hbar\omega_0$  is the smoothing range and

$$\zeta(x) = \frac{1}{\sqrt{\pi}} \exp(-x^2) \sum_{k=0}^m a_{2k} H_{2k}(x) \quad (23)$$

is the smoothing function. This work takes  $m = 3$  as the summing limit, which corresponds to the so-called plateau condition. The sought smoothed energy  $\tilde{U}$  is finally obtained as

$$\tilde{U}_{p,n} = 2 \int_{-\infty}^{\tilde{\lambda}_{p,n}} \tilde{g}_{p,n}(\epsilon) \epsilon d\epsilon. \quad (24)$$

Integration goes up to the smoothed Fermi level  $\tilde{\lambda}_{p,n}$  which is obtained from the particle number conservation for protons and neutrons. At this point the statical value of the fission barrier is available as the sum of macroscopic and microscopic energies, as in Eq. (1). This value is deformation dependent, thus, at every distance between the centers of the fragments, one has a certain energy value. The whole range of these values constitutes the final fission barrier. The advantage of this binary procedure developed here is that one can follow a certain fission channel, with a previously determined heavy-light pair of fragments.

### III. FISSION DYNAMICS

The Wentzel-Kramers-Brillouin (WKB) procedure is employed to find the possible fission paths. Thus, in order to complete the dynamics, the mass tensor  $B$  must be introduced. This work uses the binary Werner-Wheeler method, which is based on the concept of irrotational flow [37]. This procedure has been adapted for a multidimensional space of deformation: the two ratios of the spheroid semiaxes  $\chi_H = b_H/a_H$  and  $\chi_L = b_L/a_L$ , for the heavy and light fragments, the small semiaxis of the light fragment  $b_L$ , and the distance between centers  $R$ . In this way one has the total inertia  $B = B(b_L, \chi_L, \chi_H; R)$ . When one impose an arbitrary tensor

contraction on the  $R$  direction, one can assume a function  $B(R)$ :

$$\begin{aligned}
 & B(b_L(R), \chi_H(R), \chi_L(R); R) \\
 &= B_{b_L b_L} \left( \frac{db_L}{dR} \right)^2 + 2B_{b_L \chi_H} \frac{db_L}{dR} \frac{d\chi_H}{dR} \\
 &+ 2B_{b_L \chi_L} \frac{db_L}{dR} \frac{d\chi_L}{dR} + 2B_{b_L R} \frac{db_L}{dR} \\
 &+ B_{\chi_H \chi_H} \left( \frac{d\chi_H}{dR} \right)^2 + 2B_{\chi_H \chi_L} \frac{d\chi_H}{dR} \frac{d\chi_L}{dR} + 2B_{\chi_H R} \frac{d\chi_H}{dR} \\
 &+ B_{\chi_L \chi_L} \left( \frac{d\chi_L}{dR} \right)^2 + 2B_{\chi_L R} \frac{d\chi_L}{dR} + B_{RR}. \quad (25)
 \end{aligned}$$

The functions  $B_L(R)$ ,  $\chi_H(R)$ , and  $\chi_L(R)$  can be chosen in any possible way, provided that at the end of the process they take the final values corresponding to the separated values. The tensor components are defined as

$$B_{ij} = \pi \sigma_m \int_{z_{\min}}^{z_{\max}} T_{ij}(z; b_L, \chi_L, \chi_H; R) dz, \quad (26)$$

where

$$T_{ij}(z; q) = \rho_s^2(z; q) \left[ X_i(z) X_j(z) + \frac{1}{8} \rho_s^2(z; q) \frac{\partial X_i}{\partial z} \frac{\partial X_j}{\partial z} \right]. \quad (27)$$

Here  $\sigma_m$  is the nucleus mass density, and  $\rho_s^2(z; q)$  is the binary nuclear surface equation. The advantage of the procedure is that the  $X_i$  terms are only geometry dependent:

$$X_i^{(H,L)} = -\frac{1}{\rho_s^2(z; q)} \frac{\partial}{\partial q_i} \int_{z_{\min}, z_s}^{z_s, z_{\max}} \rho_s^2(z'; q) dz'. \quad (28)$$

The peculiar character of this kind of calculation in the present case is the application of formulas separately for the heavy and light parts of the overlapping region of the fission configuration. The final quantity is obtained by summing the two values:

$$X_i = X_i^{(H)} + X_i^{(L)}. \quad (29)$$

The mass tensor  $B(b_L, \chi_L, \chi_H; R)$  is calculated for all possible geometric parameters mentioned above, along the whole deformation from parent up to separated fragments. At this point, the penetrability  $P_{\text{fis}}$  can be calculated for every available path within the multidimensional space of deformation:

$$P_{\text{fis}} = \exp[-K_{\text{fis}}(b_L, \chi_H, \chi_L; R)] \quad (30)$$

with

$$\begin{aligned}
 K_{\text{fis}}(b_L, \chi_H, \chi_L; R) &= \frac{2}{\hbar} \int_{(\text{fis})} [2B(b_L(R), \chi_L(R), \\
 &\times \chi_H(R); R) E_b(R)]^{1/2} dR. \quad (31)
 \end{aligned}$$

After all possible points in this multidimensional space are covered, the minimization of the action integral  $K_{\text{fis}}$  follows. It will provide the final fission path within  $(b_L, \chi_L, \chi_H; R)$  space for a given fission channel  $(A_H, Z_H; A_L, Z_L)$ . Then all possible combinations of mass and charge asymmetry are taken into account for the initial parent nucleus.

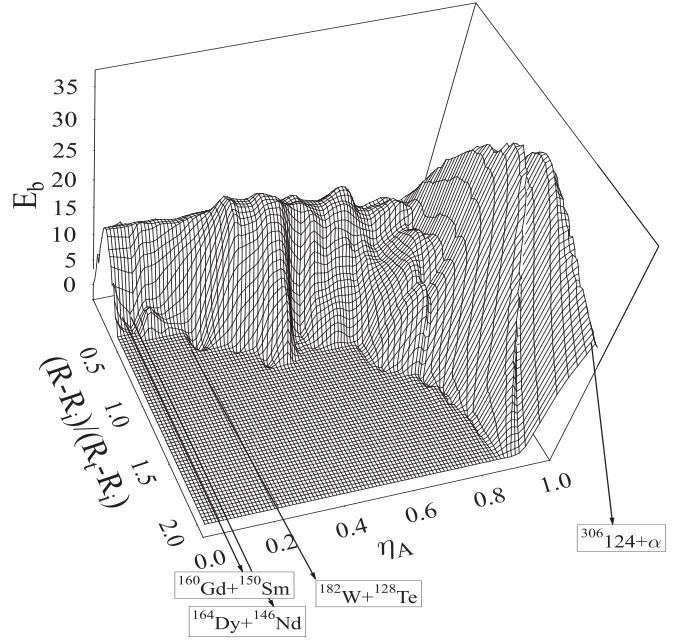


FIG. 1. Potential energy surface as a function of mass asymmetry  $\eta_A$  and reduced distance between centers  $(R - R_i)/(R_f - R_i)$  for the superheavy nucleus  $^{310}_{126}$ . Favorable fission channels are emphasized.

The lifetime calculation follows the usual formula for spontaneous fission:

$$T = \frac{\hbar \ln 2}{2} \frac{1}{E_\nu P_{\text{fis}}}, \quad (32)$$

where  $E_\nu$  is the zero point vibration energy and  $\nu$  is the assault frequency. After numerical computation, the logarithm of spontaneous fission lifetime is obtained as

$$\lg T_{sf} = -20.54 + \lg [1 + \exp 2K_{\text{fis}}] - \lg (2E_\nu), \quad (33)$$

where the zero point vibration energy  $E_\nu$  is taken as 0.7 MeV.

#### IV. DISCUSSION OF THE RESULTS

A possibly stable superheavy nucleus could be found at  $Z = 126$ ,  $N = 184$ . This proton-neutron pair has been advanced many times as a center of stability within the superheavy region in Refs. [11,13,15,17,26], among others. The binary multidimensional method previously presented is applied to  $^{310}_{126}$  for all possible fission channels, starting with alpha emission up to symmetrical decay. The spin-orbit and  $\hat{l}^2$  potentials determine the local energy minimum leading to a stable ground state. Changing these potentials is the results of different strength parameters  $\kappa$  and  $\mu$ . For  $^{310}_{126}$  one finds  $\kappa_p = 0.055$  and  $\mu_p = 0.400$  for the local proton quantum well  $Z = 126$ , and  $\kappa_n = 0.045$  and  $\mu_n = 0.400$  for the neutron one  $N = 184$ , where significant negative shell corrections have been calculated.

The deformation energy calculations for the entire range of mass asymmetry  $\eta_A = (A_H - A_L)/A$  are presented as a potential energy surface for  $^{310}_{126}$  in Fig. 1. The fission barriers are displayed as a function of  $\eta_A$  and the reduced

distance between centers  $(R - R_i)/(R_t - R_i)$ , where  $R_i$  and  $R_t$  are the initial and touching point values. Valleys are visible in quasymmetric mass reactions as well as at the extreme of alpha decay. Some favorable channels are emphasized in the figure. In the mass symmetry region two fission channels are promising as far as the picture shows:  $^{160}\text{Gd} + ^{150}\text{Sm}$  and  $^{164}\text{Dy} + ^{146}\text{Nd}$ . A more asymmetric channel is visible at the mass asymmetry corresponding to the  $^{182}\text{W} + ^{128}\text{Te}$  pair. The much more remote channel of alpha decay carves another valley within the potential energy surface. The first observation is that symmetric channels have a much shorter fission barrier. The exit point in this region is at a reduced distance between centers of  $(R - R_i)/(R_t - R_i) \approx 0.45$ . This fact means that the barrier ends while the two fragments are still partially overlapped. It is a particular feature for superheavy nuclei, mentioned also for one-center potentials, as in [9]. Within the two-center nuclear shell model, this means that at such a rather short distance between centers the fragment single-particle structures are already formed, for mass symmetric fission reactions. In contrast for the extreme mass asymmetry channel of alpha decay, the barrier goes well beyond the touching point. This characteristic is common for the alpha emission barrier from heavy nuclei, not only for superheavies. It is due to the finite range of the nuclear forces taken into account through the Yukawa-plus-exponential potential, as explained later.

The potential energy surface is obtained by minimizing the action integral within the multidimensional space of deformation, as a result of the next step, the introduction of the mass tensor components. The action integral thus obtained allows the calculation of the penetrabilities by the WKB procedure. At this point, note that a large number of similar calculations use only the constant reduced mass  $\mu_A = (A_H - A_L)/A$ , instead of the deformation dependent inertia  $B(b_L, \chi_L, \chi_H)$ . The results differ by orders of magnitude, affecting the lifetime predictions. The comparison between penetrability logarithms calculated with  $B(b_L, \chi_L, \chi_H)$  and  $\mu_A$  (not to be mistaken for the  $\hat{I}^2$  strength parameter  $\mu$ ), are presented in Fig. 2, for the whole range of mass asymmetry. Differences go up to ten orders of magnitude. The reduced mass (dotted line) produces always lower values of penetrability. The highest values are obtained for mass symmetric fission channels. A maximum appears at  $^{164}\text{Dy} + ^{146}\text{Nd}$ , followed by  $^{160}\text{Gd} + ^{150}\text{Sm}$ . The Coulomb repulsion has a main role here, since it is maximized at symmetric fragment charges, compensating the finite range Yukawa forces which stabilize the system. Another comparable maximum in penetrability appears at  $^{182}\text{W} + ^{128}\text{Te}$ . Then the next peak is obviously evidenced for the alpha decay channel. The particular feature for alpha decay is that it appears within an abrupt change of behavior of the penetrability. All other channels neighboring the alpha emission have much lower probability. This is certainly due to the very strong bound of the two-proton-two-neutron configuration, namely a very deep, negative shell correction energy. The shell correction value added to the total energy for alpha decay is  $-12.3$  MeV, which drastically lowers the macroscopic barrier.

The corresponding effect on the half-life behavior for spontaneous fission channels as a function of mass asymmetry is presented in Fig. 3. The dotted line displays the half-lives

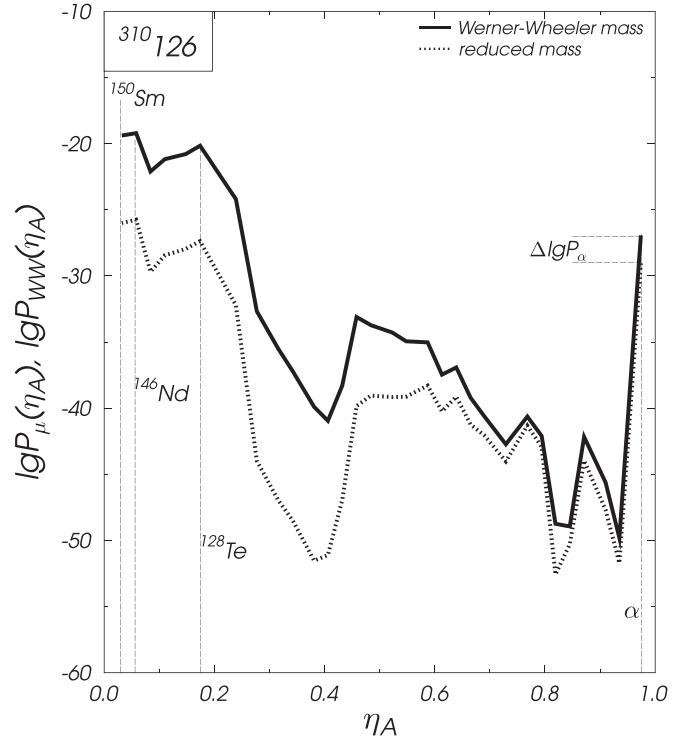


FIG. 2. Logarithm of penetrability for reduced mass,  $\lg P_\mu$ , and Werner-Wheeler,  $\lg T_{\text{WW}}^{\text{sf}}$ , mass inertia calculations, for the decay of  $^{310}\text{126}$  as a function of mass asymmetry  $\eta_A$ . Favored fission channels and alpha decay differences are mentioned, due to the two kinds of calculations.

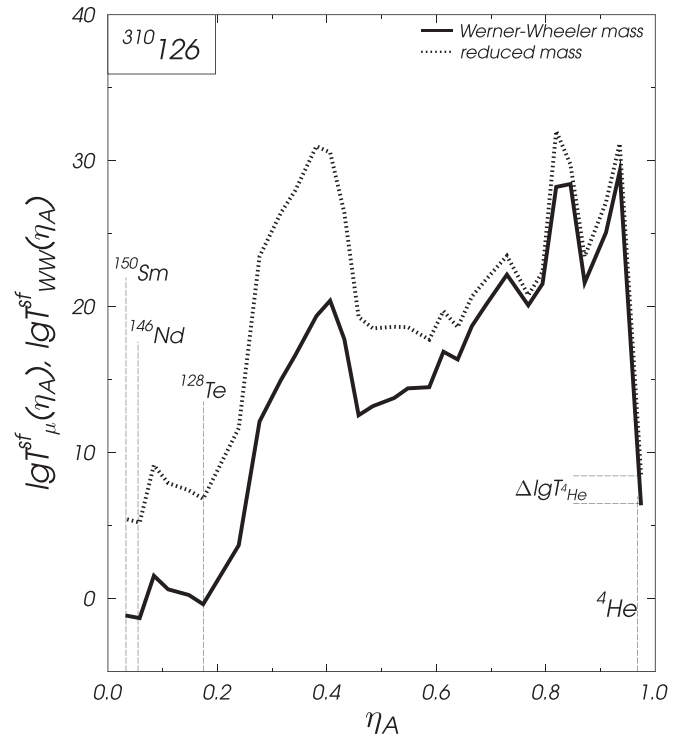


FIG. 3. Logarithm of half-life for reduced mass,  $\lg T_\mu^{\text{sf}}$ , and Werner-Wheeler,  $\lg T_{\text{WW}}^{\text{sf}}$ , mass inertia calculations, for the decay of  $^{310}\text{126}$ , as a function of mass asymmetry  $\eta_A$ . Quasisymmetric favored fission channels as well as the alpha decay one are presented.

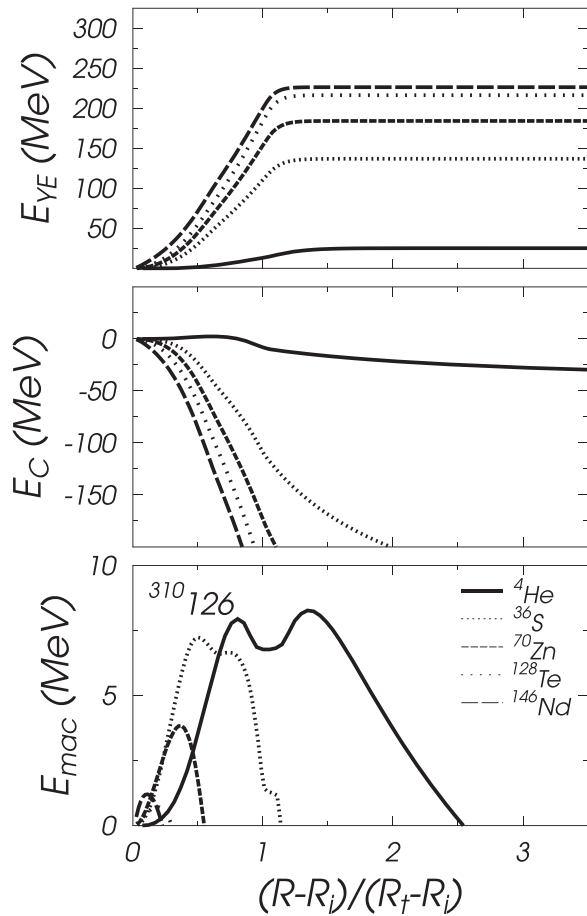


FIG. 4. Contribution of the macroscopic terms to the liquid drop energy for five emitted fragments from  $^{310}126$ . The Yukawa-plus-exponential term ( $E_{YE}$ ) in the upper plot shows increasing values as one moves to more symmetric reactions. The Coulomb term ( $E_C$ ) abruptly decreases for heavy fragment emission, but varies softly for alpha decay (middle plot). The total macroscopic barrier ( $E_{mac}$ ) shows the largest values for alpha decay.

calculated with the reduced mass  $\mu$ , whereas the full line displays the complete dynamics with the Werner-Wheeler (WW) mass tensor. The lowest values are visible in the symmetrical region of mass division. Minimum peaks appear for  $^{164}\text{Dy} + ^{146}\text{Nd}$ ,  $^{160}\text{Gd} + ^{150}\text{Sm}$ , and for the quasisymmetrical  $^{182}\text{W} + ^{128}\text{Te}$  reactions, corresponding to the highest penetrabilities. It is worthwhile to mention the different behaviors for the two kinds of calculation. Within the reduced mass line, the alpha decay half-life is almost equal to the symmetrical splitting one. When calculations are performed with the Werner-Wheeler mass tensor, the mass symmetrical reaction produces a half-life about eight orders of magnitude lower. Even the difference between alpha half-lives with  $\mu$  and WW calculations,  $\Delta \lg T_{4\text{He}}$ , is of 2.3 orders of magnitude. Such differences between  $\mu$  and WW calculations are further analyzed.

The shape of the barrier is determined by the macroscopic and microscopic energies. The macroscopic one is formed by the Coulomb and nuclear surface terms, of the Yukawa-plus-exponential (Y + E) type. An explanatory plot is presented

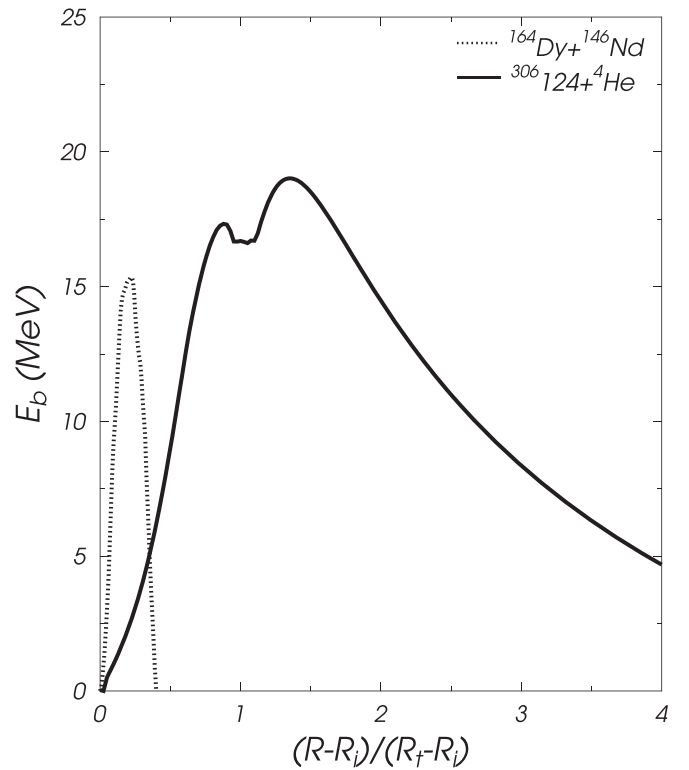


FIG. 5. Fission barriers for quasisymmetric  $^{146}\text{Nd}$  emission and alpha decay, as a function of the reduced distance between centers,  $(R - R_i)/(R_f - R_i)$ . The shape of the barriers would suggest a much larger half-life for alpha decay than for any other channel (large and high barrier), without the influence of the inertia tensor.

in Fig. 4. The balance between the two macroscopic terms is emphasized for five different reactions, increasing the light fragment proton number from alpha up to  $^{146}\text{Nd}$  emission. The nuclear surface term  $E_{YE}$  (upper plot) increases until little after the touching point, due to the finite range of the nuclear forces. After that, this term is constant, equal to the two separated fragment values. The Coulomb term (middle plot), scaled to the initial sphere value, abruptly decreases. The smoother decrease is for alpha decay. Though at a lower level, the surface Y + E energy overcomes the Coulomb term at a longer distance between centers for alpha decay. At the same distances, the Coulomb term for more symmetric reactions is much lower, decreasing the total macroscopic value of the barrier. The final Y + E energies are shown on the lower plot. There is a drastic decrease of the macroscopic barrier as the charge asymmetry decreases and the reaction becomes more symmetric. The difference between the Y + E and total barriers is due to the shell effects.

In Fig. 5 the fission barriers are displayed for two major competitors for the decay of  $^{310}126$ . The barrier of the symmetric channel  $^{164}\text{Dy} + ^{146}\text{Nd}$  is extremely narrow. Its height of almost 15.2 MeV does not compensate for its width. The exit point for this barrier is at a reduced distance between centers of less than 0.5. Note that the touching point is at value 1. That means a scission point exists inside the overlapping region, on the steep decline of the total deformation energy.

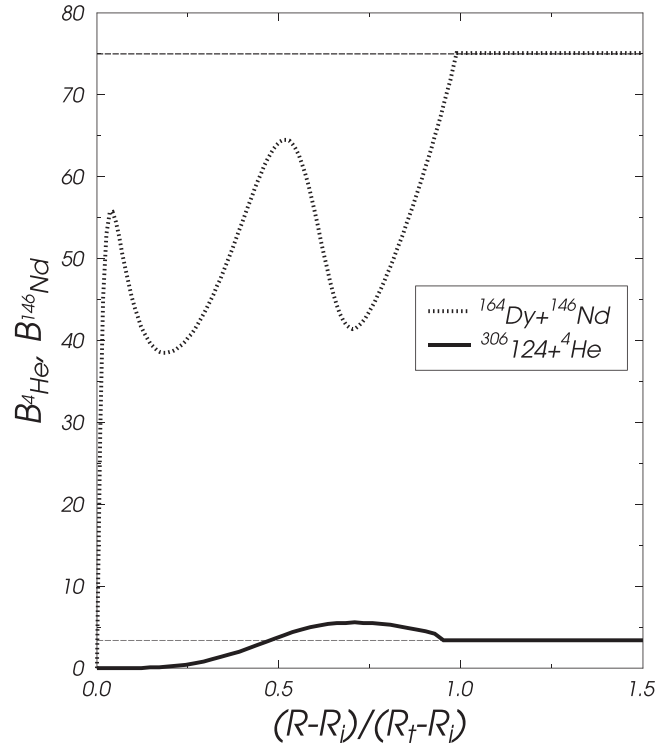


FIG. 6. Mass inertia for alpha decay,  $B_{4\text{He}}$ , and for  $^{146}\text{Nd}$  emission,  $B_{^{146}\text{Nd}}$ . The horizontal dotted lines are the reduced masses for the two reactions.

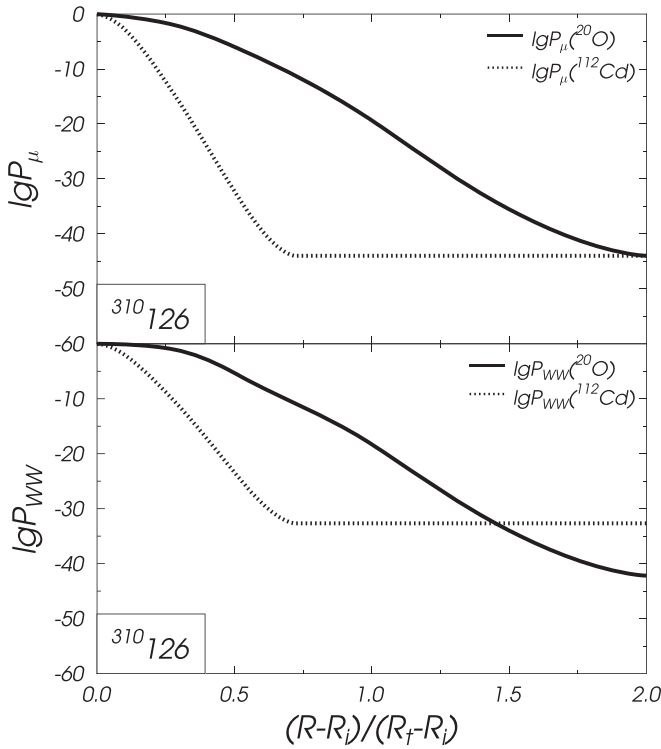


FIG. 7. Logarithms of penetrability for two fission channels which have same value when calculated with the reduced mass (upper plot) and differ when calculated with the Werner-Wheeler inertia (lower plot).

TABLE I. Logarithms of penetrability and fission lifetime with reduced mass,  $\lg P_\mu$  and  $\lg T_\mu$ , and with Werner-Wheeler mass tensor calculations,  $\lg P_{\text{WW}}$  and  $\lg T_{\text{WW}}$ .

Reaction	$\lg P_\mu$	$\lg P_{\text{WW}}$	$\lg T_\mu$	$\lg T_{\text{WW}}$
$^{160}\text{Gd} + ^{150}\text{Sm}$	-25.99	-19.38	5.46	-1.16
$^{164}\text{Dy} + ^{146}\text{Nd}$	-25.74	-19.2	5.20	-1.34
$^{168}\text{Er} + ^{142}\text{Ce}$	-29.68	-22.1	9.14	1.56
$^{172}\text{Yb} + ^{138}\text{Ba}$	-28.44	-21.17	7.91	0.63
$^{178}\text{Hf} + ^{132}\text{Xe}$	-27.95	-20.78	7.41	0.24
$^{182}\text{W} + ^{128}\text{Te}$	-27.37	-20.15	6.83	-0.39
$^{192}\text{Os} + ^{118}\text{Sn}$	-32.21	-24.19	11.67	3.65
$^{198}\text{Pt} + ^{112}\text{Cd}$	-43.98	-32.67	23.44	12.12
$^{204}\text{Hg} + ^{106}\text{Pd}$	-46.97	-35.51	26.43	14.97
$^{208}\text{Pb} + ^{102}\text{Ru}$	-48.48	-37.19	27.94	16.65
$^{214}\text{Po} + ^{96}\text{Mo}$	-51.53	-39.9	30.99	19.36
$^{218}\text{Rn} + ^{92}\text{Zr}$	-51.11	-40.95	30.56	20.41
$^{222}\text{Ra} + ^{88}\text{Sr}$	-46.95	-38.3	26.42	17.76
$^{226}\text{Th} + ^{84}\text{Kr}$	-39.83	-33.1	19.29	12.56
$^{230}\text{U} + ^{80}\text{Se}$	-39.05	-33.72	18.51	13.18
$^{236}\text{Pu} + ^{74}\text{Ge}$	-39.16	-34.28	18.62	13.74
$^{240}\text{Cm} + ^{70}\text{Zn}$	-39.13	-34.94	18.59	14.4
$^{246}\text{Cf} + ^{64}\text{Ni}$	-38.29	-35.02	17.74	14.48
$^{250}\text{Fm} + ^{60}\text{Fe}$	-40.24	-37.46	19.70	16.91
$^{254}\text{No} + ^{56}\text{Cr}$	-39.13	36.92	18.59	16.38
$^{258}\text{Rf} + ^{52}\text{Ti}$	-41.23	-39.21	20.69	18.67
$^{262}\text{Sg} + ^{48}\text{Ca}$	-42.06	-40.62	21.82	20.08
$^{268}\text{Hs} + ^{42}\text{Ar}$	-44.02	-42.73	23.48	22.19
$^{274}\text{Ds} + ^{36}\text{S}$	-41.32	-40.63	20.78	20.08
$^{278}\text{Cn} + ^{32}\text{Si}$	-42.92	-42.1	22.38	21.56
$^{282}\text{Fl} + ^{28}\text{Mg}$	-52.57	-48.74	32.03	28.2
$^{286}\text{Lv} + ^{24}\text{Ne}$	-50.29	-48.94	29.76	28.4
$^{290}\text{118} + ^{20}\text{O}$	-43.97	-42.17	23.43	21.64
$^{296}\text{120} + ^{14}\text{C}$	-47.69	-45.62	27.15	25.08
$^{300}\text{122} + ^{10}\text{Be}$	-51.71	-49.8	31.17	29.06
$^{306}\text{124} + ^4\text{He}$	-29.04	-26.93	8.5	6.39

In contrast, the alpha decay barrier (full line) goes way beyond the touching point, displaying an extremely large width together with its 17.4 MeV maximum height. Based only on this picture, one would expect a much larger half-life for alpha decay than for any other fission channel. Consequently, there must be a quantitative compensation in the WKB calculation for alpha decay. The reason for such a drastic change in half-life is presented in Fig. 6. The variation of the Werner-Wheeler total mass tensor  $B_i$ , contracted along the distance between centers, versus the reduced distance is presented for the quasysymmetrical fission channel  $^{164}\text{Dy} + ^{146}\text{Nd}$  (dotted line) and for alpha decay (full line). The straight horizontal lines are the reduced mass  $\mu$  values. For alpha emission, what one gains in lower than  $\mu$  inertia  $B_i$  values up to 0.5 reduced distance, one loses in penetrability because of higher than  $\mu$  values from 0.5 to 1. Nevertheless, even such small difference in inertia produces the gap  $\Delta \lg T_{4\text{He}}$  mentioned above. The WW mass inertia variation for  $^{146}\text{Nd}$  emission has lower values all along the deformation path. This negative difference against the reduced mass produces the lowest action integral, making the symmetrical channels competitive against alpha decay.

The direct effect of the mass tensor versus reduced mass difference upon the penetrability is shown in Fig. 7, where the same two fission channels are analyzed within the penetrability against the reduced mass effect. The upper plot shows the penetrability logarithm  $\lg P_\mu$  calculated with the reduced mass for  $^{20}\text{O}$  (full line) and  $^{112}\text{Cd}$  (dotted line) emission. What one can observe is that, despite a different fission path, both reactions end up at the same value of  $\lg P_\mu$ . The same reactions are calculated with the Werner-Wheeler mass tensor ( $\lg P_{\text{WW}}$ , lower plot). The difference of ten orders of magnitude in the final values is obvious, making the more symmetric  $^{112}\text{Cd}$  emission favorable.

All possible mass asymmetries have been calculated, from symmetry up to totally asymmetric alpha decay from  $^{310}126$ . The numerical results are presented in Table I. Logarithms of the penetrabilities and fission lifetimes are displayed for Werner-Wheeler and reduced mass type approaches. The differences in penetrability are reflected in half-life values. Mass tensor dependent calculations produce six to eleven orders of magnitude difference in half-life. The most remarkable reactions are in the symmetrical mass division region. Emission of  $^{150}\text{Sm}$ ,  $^{146}\text{Nd}$ , and  $^{128}\text{Te}$  display a favored way of decay versus alpha emission, though this asymmetrical channel has an obvious half-life minimum.

## V. CONCLUSIONS

The binary macroscopic-microscopic method has been developed for the calculation of fission barriers. The use of the deformed two-center shell model ensures the passage of the microscopic corrections from the parent quantum well through the partially overlapped binary deformed potentials, up to final separated fragments. The dynamics of the process has been completed with the use of the Werner-Wheeler mass inertia specialized in binary shape configurations. The calculations applied to the decay of the presumed doubly magic  $^{310}126$  show favored symmetric fission channels for  $^{146}\text{Nd}$ ,  $^{150}\text{Sm}$ , and  $^{128}\text{Te}$  versus alpha emission. The results also display a minimum for alpha decay half-life, but less probable than mass symmetrical reactions, when the mass inertia is used instead of the reduced mass in the dynamics.

## ACKNOWLEDGMENTS

This work is supported by The Ministry of Research, Innovation and Digitalization, Romania, through the Nucleu Program 2023, and by the Frankfurt Institute for Advanced Studies, Frankfurt am Main, Germany.

- 
- [1] C. M. Folden III, S. L. Nelson, C. E. Dullmann, J. M. Schwantes, R. Sudowe, C. M. Zielinski, K. E. Gregorich, H. Nitsche, and D. C. Hoffman, Excitation function for the production of  $^{262}\text{Bh}$  ( $Z = 107$ ) in the odd- $Z$  projectile reaction  $^{208}\text{Pb}(^{55}\text{Mn}, n)$ , *Phys. Rev. C* **73**, 014611 (2006).
- [2] Yu. Oganessian *et al.*, Experiments on the synthesis of element 107, *JETP Lett.* **20**, 265 (1974).
- [3] S. Hofmann, Synthesis of superheavy elements by cold fusion, *Radiochim. Acta* **99**, 405 (2011).
- [4] P. Armbruster, On the production of superheavy elements, *Annu. Rev. Nucl. Part. Sci.* **50**, 411 (2000).
- [5] K. Morita *et al.*, Experiment on the synthesis of element 113 in the reaction  $^{209}\text{Bi}(^{70}\text{Zn}, n)^{278}113$ , *J. Phys. Soc. Jpn.* **73**, 2593 (2004).
- [6] P. Hodgson, Discovery of superheavy elements, *Nature (London)* **261**, 627 (1976).
- [7] V. M. Strutinsky, Shell effects in nuclear masses and deformation energies, *Nucl. Phys. A* **95**, 420 (1967).
- [8] S. Cwiok and A. Sobiczewski, Potential energy and fission barriers of superheavy nuclei calculated in multidimensional deformation space, *Z. Phys. A* **342**, 203 (1992).
- [9] R. Smolanczuk, J. Skalski, and A. Sobiczewski, Spontaneous-fission half-lives of deformed superheavy nuclei, *Phys. Rev. C* **52**, 1871 (1995).
- [10] J. J. Li, W. H. Long, J. Margueron, and N. Van Giai, Relativistic Hartree-Fock Bogoliubov predictions of superheavy magic nuclei, *J. Phys.: Conf. Series* **580**, 012006 (2015).
- [11] K. Rutz, M. Bender, T. Burvenich, T. Schilling, P.-G. Reinhard, J. A. Maruhn and W. Greiner, Superheavy nuclei in self-consistent nuclear calculations, *Phys. Rev. C* **56**, 238 (1997).
- [12] J. J. Li, W. H. Long, J. Margueron, and N. V. Giai, Superheavy magic structures in the relativistic Hartree-Fock-Bogoliubov approach, *Phys. Lett.* **732**, 169 (2014).
- [13] W. Zhe-Ying, X. Fu-Rong, Z. En-Guang, and Z. Chun-Kai, Spherical and Deformed shell closures in superheavy nuclei, *Chin. Phys. Lett.* **20**, 1702 (2003).
- [14] A. Sobiczewski, F. Gareev, and B. N. Kalinkin, Closed shells for  $Z > 82$  and  $N > 126$  in a diffuse potential well, *Phys. Lett.* **22**, 500 (1966).
- [15] H. Meldner, Predictions of new magic regions and masses for superheavy nuclei from calculations with realistic shell model single particle Hamiltonians, *Ark. Fys.* **36**, 593 (1967).
- [16] M. Bender and P.-H. Heenen, Structure of superheavy nuclei, *J. Phys.: Conf. Ser.* **420**, 012002 (2013).
- [17] S. Liran, A. Marinov, and N. Zeldes, Semiempirical shell model masses with magic number  $Z = 126$  for superheavy elements, *Phys. Rev. C* **62**, 047301 (2000).
- [18] S. Kumar, M. Balasubramaniam, R. K. Gupta, G. Muenzenberg and W. Greiner, The formation and decay of superheavy nuclei produced in  $^{48}\text{Ca}$ -induced reactions, *J. Phys. G: Nucl. Part. Phys.* **29**, 625 (2003).
- [19] G. Royer, Alpha emission and spontaneous fission through quasi-molecular shapes, *J. Phys. G: Nucl. Part. Phys.* **26**, 1149 (2000).
- [20] K. P. Santhosh, C. Nithya, and T. A. Jose, Decay modes of superheavy nuclei using a modified generalized liquid drop model and a mass-inertia dependent approach for spontaneous fission, *Phys. Rev. C* **104**, 024617 (2021).
- [21] I. Muntian and A. Sobiczewski, *Fission barriers of heavy and superheavy nuclei*, in *Structure and Dynamics of Elementary Matter*, edited by W. Greiner and M. G. Itkis, NATO Science Series Vol. 166 (Springer, Dodrecht, 2004).
- [22] T. Burvenich, M. Bender, P.-G. Reinhard, and J. A. Maruhn, Fission barriers of superheavy nuclei from

- self-consistent mean-field models, *Acta Phys. Hungarica A* **16**, 275 (2002).
- [23] L. Hong-Feng, G. Li-Sheng, and M. Jie, Fission barrier for  $^{240}\text{Pu}$  in the quadrupole constrained relativistic mean field approach, *Chin. Phys. Lett.* **23**, 2940 (2006).
- [24] H. C. Manjunatha, Alpha decay properties of superheavy nuclei  $Z = 126$ , *Nucl. Phys. A* **945**, 42 (2016).
- [25] A. M. Nagaraja, H. C. Manjunatha, N. Sowmya, L. Seenappa, P. S. Damodara Gupta, N. Manjunatha, and S. Alfred Cecil Raj, Heavy particle radioactivity of superheavy element  $Z = 126$ , *Nucl. Phys. A* **1015**, 122306 (2021).
- [26] G. Naveya, S. Santosh Kumar, and A. Stephen, A systematic study on  $\alpha$ -decay chains of superheavy nuclei  $Z = 126, 138$ , *Int. J. Mod. Phys. E* **29**, 2050034 (2020).
- [27] K. Pomorski *et al.*, On the stability of superheavy nuclei, *Eur. Phys. J. A* **58**, 77 (2022).
- [28] R. A. Gherghescu and D. N. Poenaru, Fission channels for fragment isotopes from  $^{298}\text{Fl}$  with magic nucleon numbers, *Phys. Rev. C* **106**, 034611 (2022).
- [29] W. J. Cody, Chebyshev approximations for the complete elliptic integrals K and E, *Math. Comput.* **19**, 105 (1965).
- [30] D. N. Poenaru, M. Ivascu, and D. Mazilu, Folded Yukawa-plus-exponential model for nuclei with different charge densities, *Comput. Phys. Commun.* **19**, 205 (1980).
- [31] H. J. Krappe, J. R. Nix, and A. J. Sierk, Unified nuclear potential for heavy ion elastic scattering, fusion and ground state masses and deformations, *Phys. Rev. C* **20**, 992 (1979).
- [32] J. Maruhn and W. Greiner, The asymmetric two-center shell model, *Z. Phys. A* **251**, 431 (1972).
- [33] A. Diaz-Torres and W. Scheid, Two-center shell model with Woods-Saxon potentials: Adiabatic and diabatic states in fusion, *Nucl. Phys. A* **757**, 373 (2005).
- [34] A. Diaz-Torres, Solving the two-center nuclear shell model problem with arbitrary oriented deformed potentials, *Phys. Rev. Lett.* **101**, 122501 (2008).
- [35] R. A. Gherghescu, Deformed two-center shell model, *Phys. Rev. C* **67**, 014309 (2003).
- [36] R. A. Gherghescu and D. N. Poenaru, Fission barriers of superheavy nuclei for emitted fragment isotopes near proton magic numbers, *Phys. Rev. C* **106**, 034616 (2022).
- [37] K. T. Davies, A. J. Sierk, and J. R. Nix, Effect of viscosity on the dynamics of fission, *Phys. Rev. C* **13**, 2385 (1976).